ROM SAF Report 20
Ref: SAF/ROM/METO/REP/RSR/020
Web: www.romsaf.org
Date: 06 Feb 2015

The EUMETSAT Network of Satellite Application Facilities

ROM SAF
Radio Occultation Meteorology

ROM SAF Report 20

Interpolation artefact in ECMWF monthly standard deviation plots

Hans Gleisner

Danish Meteorological Institute

DOCUMENT AUTHOR TABLE

	Name	Function	Date	Comments
Prepared by:	Hans Gleisner	ROM SAF Project Scientist	06/02/2015	
Reviewed by:	Kent B. Lauritsen	ROM SAF Project Manager	09/02/2015	
Approved by:	Kent B. Lauritsen	ROM SAF Project Manager	10/02/2015	

DOCUMENTATION CHANGE RECORD

Issue / Revision	Date	By	Description
Version 1.0	06/02/2015	HGL	First version.

ROM SAF

The Radio Occultation Meteorology Satellite Application Facility (ROM SAF) is a decentralized centre under EUMETSAT, responsible for operational processing of GRAS radio occultation data from the Metop satellites as well as RO data from other missions. The ROM SAF delivers bending angle, refractivity, temperature, pressure, and humidity profiles in near-real time and offline for NWP and climate users. The offline profiles are further processed into climate products consisting of gridded monthly zonal means of bending angle, refractivity, temperature, humidity, and geopotential heights together with error descriptions.

The ROM SAF also maintains the Radio Occultation Processing Package (ROPP) which contains software modules that aid users wishing to process, quality-control and assimilate radio occultation data from any radio occultation mission into NWP and other models.

The ROM SAF Leading Entity is the Danish Meteorological Institute (DMI), with Cooperating Entities: i) European Centre for Medium-Range Weather Forecasts (ECMWF) in Reading, United Kingdom, ii) Institut D'Estudis Espacials de Catalunya (IEEC) in Barcelona, Spain, and iii) Met Office in Exeter, United Kingdom. To get access to our products or to read more about the project please go to http://www.romsaf.org.

Intellectual Property Rights

List of Contents

Abstract

During the development of the ROM SAF Level 3 gridded climate data processing software, a pronounced wave pattern artefact was frequently found in plots of the standard deviations of ECMWF model data. It was exclusively a problem for model data, and did not affect the observed RO data. The wave pattern was most easily discerned at low latitudes and above an altitude of 20 kilometers, and there was a seasonal variation with a tendency for the wave pattern to become stronger in the summer hemisphere.

It is here shown that the wave pattern artefact is caused by the reduction of variance at the interpolation points as a result of the weighted averaging prescribed by the interpolation from model levels to intermediate points. It does not depend on the detailed choice of interpolation function. It is also shown that the dependence of the wave pattern on latitude, altitude, and season is governed by the mixing of model levels at fixed altitudes along zonal latitude bands.

We propose to use log-spline interpolation of refractivity as a remedy for this problem. This introduces an additional source of variability at the interpolation points, which is enough to substantially reduce the problem even though it is not fundamentally resolved. The interpolated refractivity profile is also used as input to the Abel transform, at a higher vertical resolution compared to the standard bending-angle forward model. Spline interpolation is also used to interpolate ECMWF model temperature, humidity, and geopotential heights from model levels to intermediate altitudes.

The solution described in this report has been implemented in the ROM SAF Level 3 processing software, *romclim*-1.1, used in the generation of data products GRM-17,…,23, as well as plots at the ROM SAF climate monitoring web pages. The artefact described in this report, and the chosen solution, only concerns the ECMWF model data used as a reference, not the observed RO data.

1. Background

The ROM SAF Level 3 gridded climate data products consist of monthly mean Radio Occultation (RO) data in 5-degree latitude bins. The monthly mean data are delivered together with the corresponding standard deviations, data numbers, and error and uncertainty estimates. They are also provided together with the corresponding monthly means and standard deviations calculated from ECMWF short-term forecasts co-located with the observed data.

In the standard deviation plots for the ECMWF co-located data, a weak wave pattern can often be seen (Figure 1). The strength of the wave pattern varies with latitude, altitude, and season. It is most easily discerned in the bending-angle and refractivity standard deviations, but can also be seen in other geophysical variables, as well as in plots showing O-B standard deviations (i.e. plots showing standard deviations of the differences, or relative differences, between observed data and co-located ECMWF data). The corresponding plots based solely on *observed* RO data do not exhibit a similar pattern – it is exclusively a problem for plots that include *model* data.

The wave pattern is clearly an artefact, and must somehow be generated by the data processing. This short report is an attempt to explain the causes of the artefact, and to show how the magnitude of the wave pattern is reduced in the ROM SAF Level 3 processing.

2. Wave pattern artefact

We here describe the wave pattern artefact as it appeared during January 2011. It is very similar for other months, with the exception of a seasonal change with latitude, where the summer hemisphere exhibits a more pronounced wave pattern. We use observed data from the COSMIC mission, binned into 5-degree latitude bands, and background data from ECMWF short-term forecasts, which during this period were provided on 91 model levels ranging from the surface up to 0.01 hPa.

Figure 1 shows the bending-angle and refractivity standard deviations of the ECMWF short-term forecasts co-located with the COSMIC observations, forward-modelled from model parameters to observation space using the standard *ROPP*-6.1 routines. There is clearly a wave pattern at low latitudes and above an altitude of 20 kilometers. There is also a seasonal variation (not shown here) with a tendency for the wave pattern to become stronger in the summer hemisphere. The vertical wave length increases with height, and suggests some sort of relation to the ECMWF model levels. Depending on the contour plotting parameters, it is more or less easily spotted.

Figure 2 shows the refractivity standard deviations, σ_B/m_B of, the ECMWF short-term forecasts in a single equatorial latitude bin (0°N–5°N), where σ_B is given by

$$\sigma_B^2 = \frac{1}{M}\sum_{i=1}^{M}\left(N_{B,i} - m_B\right)^2 \qquad (1)$$

M is the number of data points in the bin, N_B is the ECMWF refractivity, and m_B is the average of the ECMWF refractivity in the bin (here, *B* denotes "background"). Similarly, Figure 3 shows the standard deviations, σ_{O-B}/m_B, of the differences between observations and ECMWF short-term forecasts, where σ_{O-B} is given by

$$\sigma_{O-B}^2 = \frac{1}{M}\sum_{i=1}^{M}\left((N_{O,i} - N_{B,i}) - m_{O-B}\right)^2 \qquad (2)$$

and $m_{O\text{-}B}$ is the corresponding mean (here, *O* denotes "observation"). Note that the standard deviations in Figures 1 to 3 (as well as in Figures 6 to 8) are given in relative terms.

In Figures 2 and 3, the mean altitudes of ECMWF model levels (gray, horizontal lines) are also indicated, showing the close correspondence between the wave pattern and the model levels. In Figure 2, the standard deviations exhibit local maxima at altitudes corresponding to model levels, and local minima between model levels. The standard deviations in Figure 3 show a similar tendency, but much weaker and with a less clear correspondence with the model levels. There is also tendency for the means in Figure 3, i.e. the biases of the ECMWF forecasts relative to observations, to show a wave pattern. The wave patterns in the bias plots have been described by Burrows et al. [2, 3] and shown to be a consequence of interpolation errors. This is further discussed in Section 4.

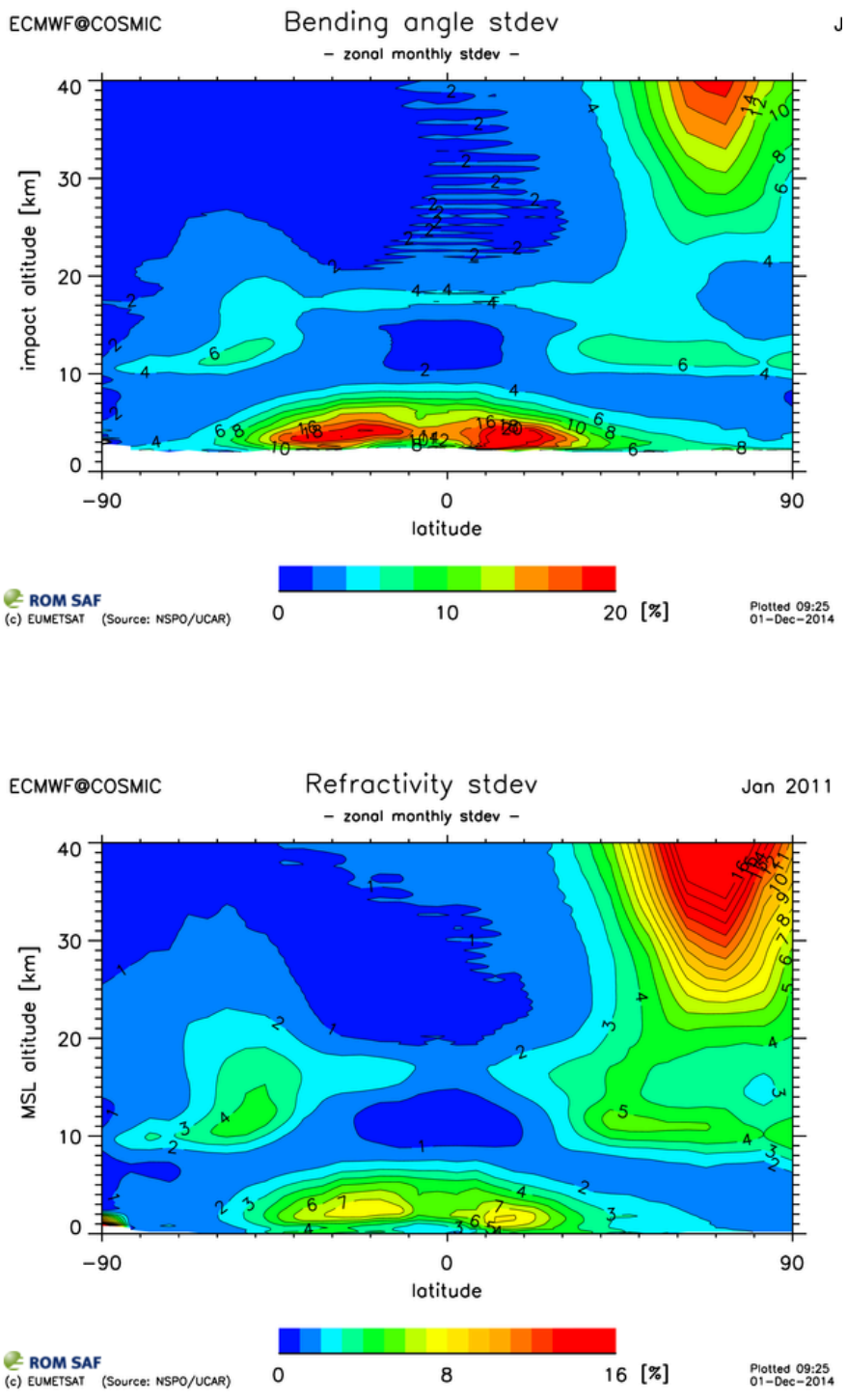

Figure 1. *Bending-angle and refractivity standard deviations of ECMWF short-term forecasts in 5-degree latitude bins, using the ROPP-6.1 forward-modelling routines. The standard deviations are quantified as a percentage relative to the corresponding monthly mean.*

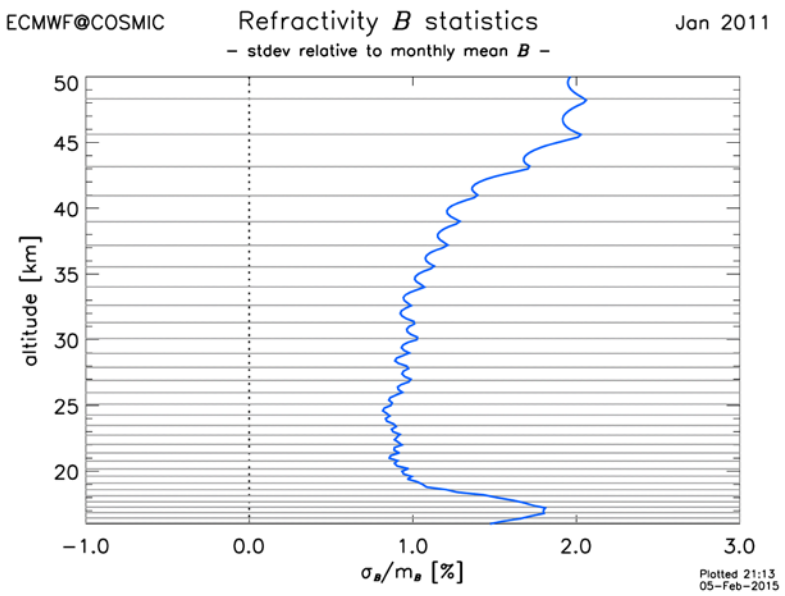

Figure 2. *Refractivity standard deviations of ECMWF short-term forecasts in an equatorial latitude bin (0°N–5°N), relative to the corresponding ECMWF monthly means. The gray, horizontal lines show mean model levels within the latitude bin. Standard deviations have local maxima at the model levels, and are smaller between the model levels.*

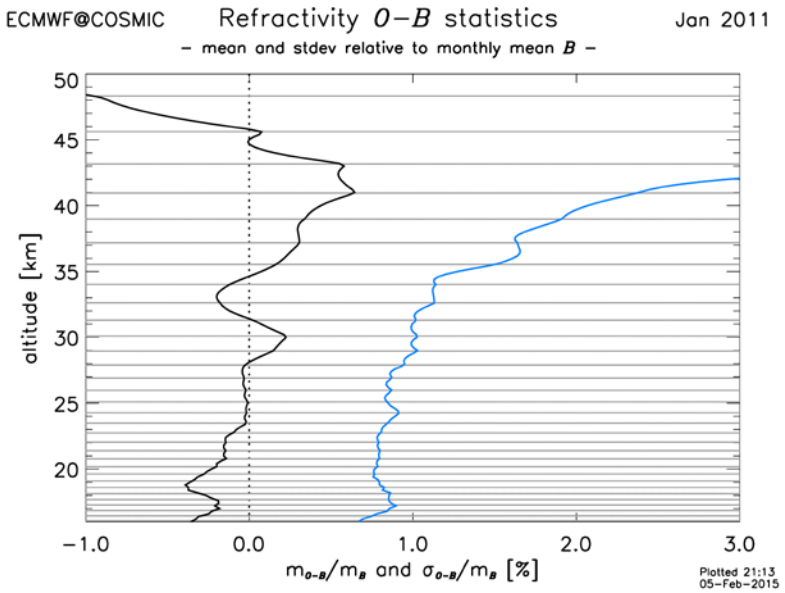

Figure 3. *Refractivity means (black line) and standard deviations (blue line) of differences between observations and ECMWF short-term forecasts in an equatorial latitude bin (0°N–5°N), relative to the corresponding ECMWF monthly means. The gray, horizontal lines show mean model levels within the latitude bin. Weak wave patterns can be discerned in both curves, but compared to Figure 2 they have a less distinct appearance.*

3. Model levels and altitudes

ECMWF model levels are defined such that there is a gradual transition from the lowest levels, which follow Earth's surface (orography), to the upper levels, which are near-constant pressure surfaces [4]. As a consequence, there is mixing of model levels at low altitudes due to the varying orography along a latitude band, and mixing of model levels at high altitudes due to the constant-pressure surfaces moving up and down in response to variability related to weather. This latter mixing is strongest in the winter hemisphere, and thus changes seasonally.

Figure 4 visualizes the mixing of model levels. For nearly 30,000 ECMWF short-term forecast profiles co-located with COSMIC data during January 2011, the model levels are indicated by small dots. Above 20 kilometers, at low latitudes and in the summer hemisphere, there is a close correspondence between model level and altitude, whereas at low altitudes and in the winter hemisphere, the model levels are strongly mixed. In the latter case, we find a whole range of model levels at any specific latitude and altitude.

We note that the regions with only marginal model-level mixing are also the regions where we find the most pronounced wave patterns. The ROM SAF statistics – averages and standard deviations – are evaluated on fixed altitudes. This means that in regions of little model-level mixing, the statistics are evaluated on nearly fixed model levels, while in regions of strong mixing, different model levels are included in the same average or standard deviation.

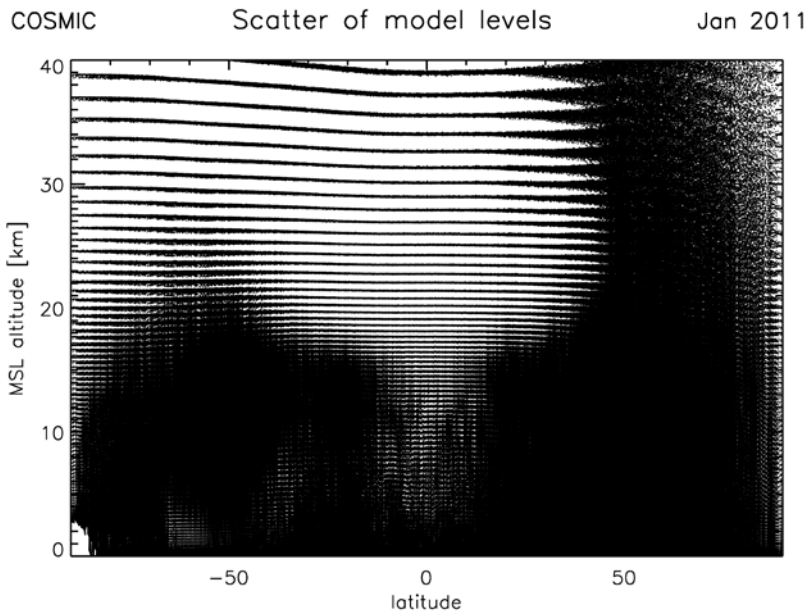

***Figure 4**. Model levels for nearly 30,000 ECMWF short-term forecast profiles. In some regions (above 20 kilometers, at low latitudes and in the summer hemisphere) there is a close correspondence between model level and altitude. In other regions, the model levels are strongly mixed: at a certain latitude and altitude we find a whole range of model levels.*

4. Cause of the wave pattern artefact

The *ROPP*-6.1 refractivity forward-modelling approach is to first evaluate refractivity at the model levels, and then do a log-linear interpolation to a denser set of intermediate altitudes [1],

$$\ln(N) = (1-a)\cdot\ln(N_i) + a\cdot\ln(N_{i+1}) \quad (3)$$

where N_i and N_{i+1} are the refractivities at model levels *i* and *i*+1, respectively, and N is the refractivity at an intermediate altitude given by the interpolation parameter

$$a = \frac{h_a - h_i}{h_{i+1} - h_i} \;;\quad a \in [0,1] \quad (4)$$

The interpolated values exhibit an *interpolation error* due to the imperfect representation of the actual variation of the refractivity between model levels. The interpolation error is zero at the model levels and attains a finite value between the model levels, hence the wave pattern in the bias plot in Figure 3. This problem was identified by Burrows et al. [2,3], and an improved form of interpolation function for refractivity was devised – still using only the two surrounding model levels (implemented in *ROPP*-8.0).

The interpolation error contributes not only to the bias m_{O-B} in Figure 3, but also to the standard deviation σ_{O-B}. In addition to this, the variances at the interpolation points are reduced compared to the model levels due to the weighted averaging prescribed by the interpolation method [5]. A proper description of interpolated *O-B* statistics must contain both these components [6]. However, for the standard deviations σ_B in Figure 2, the interpolation error in itself (i.e. the detailed choice of interpolation function) is not an issue. The wave pattern in Figure 2 is exclusively due the reduction of variance due to the weighted averaging.

We can describe the statistical effect of the weighted averaging by assuming a) that the distribution of $\ln(N)$ at a model level is Gaussian with standard deviation σ_0, and b) that the profile-to-profile variability of $\ln(N)$ is vertically uncorrelated between neighboring model levels. The latter assumption is somewhat unrealistic, but leads to a simple description. Any correlation between the model levels would act to reduce the difference in standard deviation between interpolated values and model-level values – the results described here can be considered a "worst case." With these assumptions, we can write the standard deviation as

$$\sigma = \sigma_0 \cdot \sqrt{a^2 + (1-\alpha)^2} \quad (5)$$

where σ_0 is the standard deviation at the model levels, and α is the interpolation parameter (Eq. 4). Figure 5 shows the values of the interpolated standard deviations according to this equation, with σ_0 at the model levels set to 1.0.

Hence, the fundamental cause of the wave pattern artefact in the standard deviations in Figures 1 and 2 is not the choice of interpolation function, but rather a fundamental statistical consequence of the weighted averaging prescribed by the interpolation method. Higher vertical correlations between the model levels tend to decrease the magnitude of the wave pattern. The appearance of a wave pattern in some latitude-altitude regions, and the absence in other regions, is governed by the degree of model-level mixing discussed in Section 3.

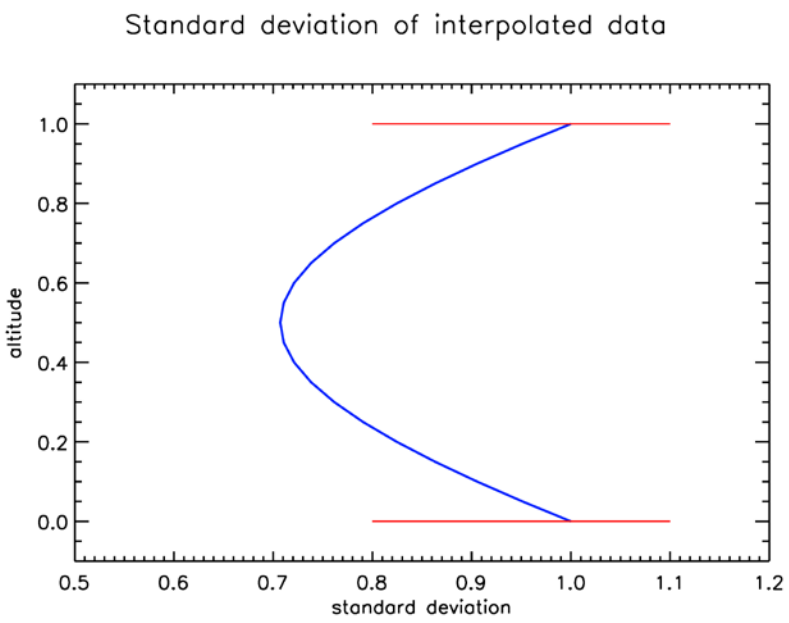

Figure 5. *Standard deviations for interpolated data assuming Gaussian distribution of data at model levels (red lines) and no vertical correlation between the model levels. The standard deviation, σ_0, at the model levels is set to 1.0.*

5. Solution

Even though the cause of the wave pattern is simple to understand, it is not obvious which the most efficient remedy for this behavior is. The simplest approach would probably be to estimate standard deviations at the model levels, and then interpolate the standard deviations rather than computing them from the interpolated values. However, this method is not straight-forward when model levels are mixed in altitude.

There is also a family of more or less complex methods that are based on determining Gaussian stochastic variables, rather than just single values, at the interpolation points [5]. Such methods would introduce a level of complexity that is not reasonable considering the marginal importance of the problem. It should be remembered that the problem discussed in the present report does not affect the observed RO data, which is the main ROM SAF Level 3 data product.

Hence, in the ROM SAF Level 3 plot procedures we have chosen to use log-spline interpolation in the refractivity forward-modelling. This type of interpolation method, which also uses data beyond the two surrounding model levels, introduces an additional source of variability. This is enough to substantially reduce the problem described in this report, even though it is not fundamentally resolved. The interpolated refractivity profile is also used as input to the Abel transform, at a higher vertical resolution compared to the standard *ROPP*-6.1 bending-angle forward model. This is described in some detail in the Appendix. The results of this alternative procedure can be seen in Figures 6 to 8, which should be compared to Figures 1 to 3.

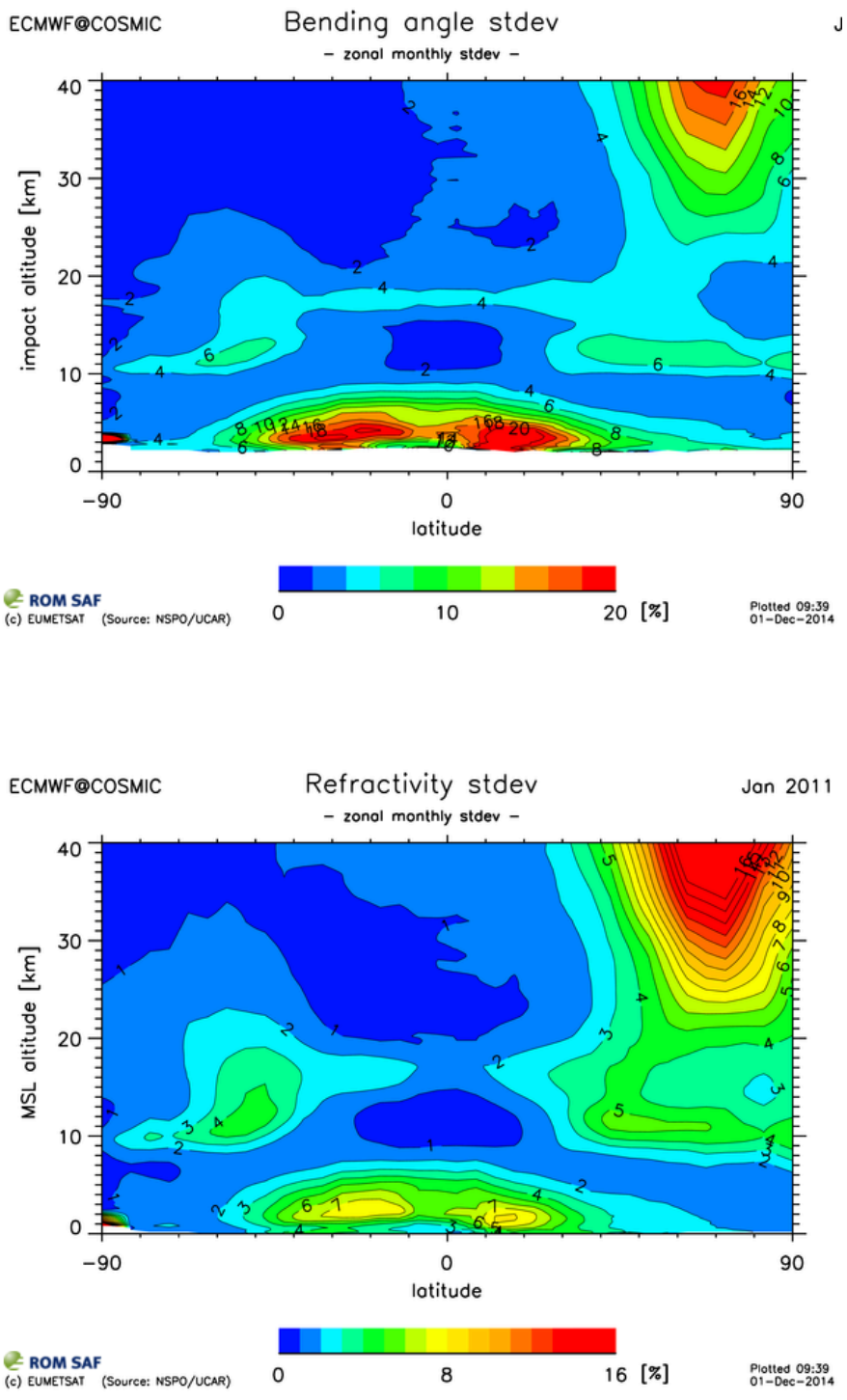

Figure 6. *Bending-angle and refractivity standard deviations of ECMWF short-term forecasts in 5-degree latitude bin. The weak wave patterns evident in Figure 1 are now largely absent as a consequence of the log-spline interpolation in the forward modelling.*

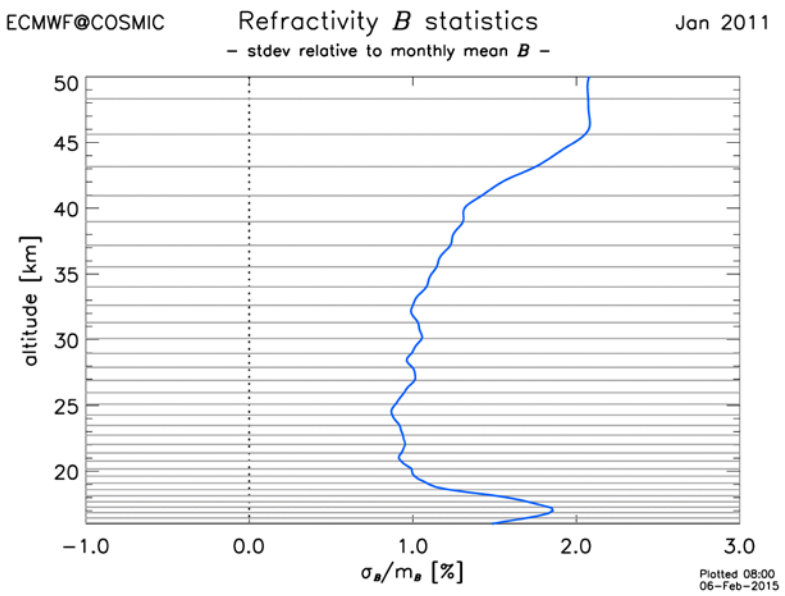

Figure 7. *Refractivity standard deviations of ECMWF short-term forecasts in an equatorial latitude bin (0°N–5°N), relative to the ECMWF corresponding monthly means. The wave pattern evident in Figure 2 is now largely absent as a consequence of the log-spline interpolation in the forward modelling.*

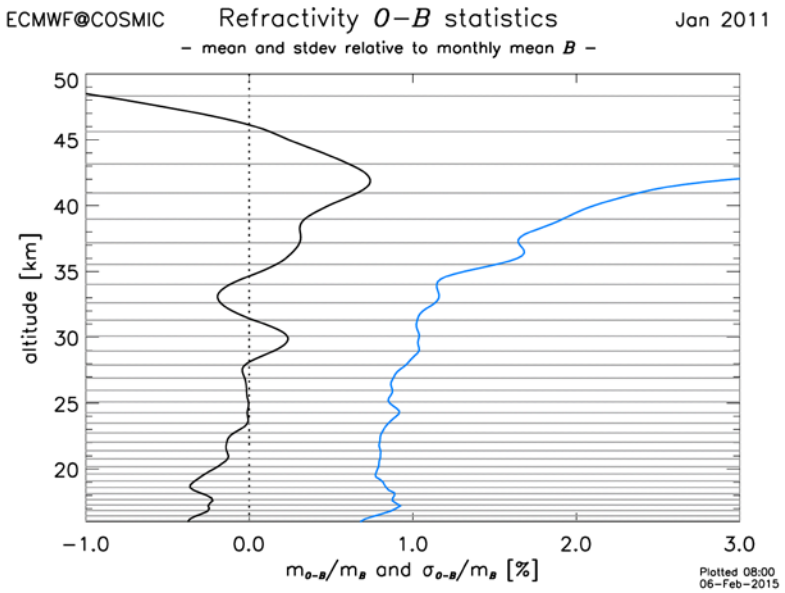

Figure 8. *Refractivity means (black line) and standard deviations (blue line) of differences between observations and ECMWF short-term forecasts in an equatorial latitude bin (0°N–5°N), relative to the corresponding ECMWF monthly means. The weak wave patterns evident in Figure 3 are now largely absent as a consequence of the log-spline interpolation in the forward modelling.*

6. Conclusions

The wave pattern artefact frequently found in plots of the standard deviations of ECMWF model data is shown to be caused by the reduction of variance at the interpolation points as a result of the weighted averaging prescribed by the interpolation from model levels to intermediate points. The appearance of a wave pattern in some latitude-altitude regions, and the absence in other regions, as well as a seasonal variation, is governed by the mixing of model levels at fixed altitudes along zonal latitude bands.

It is shown that an efficient remedy for this problem is to use a log-spline interpolation of refractivity between the model levels. This type of interpolation method introduces an additional source of variability at the interpolation points, which is enough to substantially reduce the problem even though it is not fundamentally resolved. The interpolated refractivity profile is also used as input to the Abel transform, at a higher vertical resolution compared to the standard bending-angle forward model. Spline interpolation is also used to interpolate ECMWF model temperature, humidity, and geopotential heights from model levels to intermediate altitudes.

The solution described in this report has been implemented in the ROM SAF Level 3 processing software, *romclim*-1.1, used in the generation of the data products GRM-17,…,23, as well as plots at the ROM SAF climate monitoring web pages http://www.romsaf.org/climate_monitoring. The artefact described in the present report, and the suggested solution, only concerns the ECMWF model data used as a reference, not the observed RO data.

Appendix: ROM SAF Level 3 processing

```
SUBROUTINE forward_ropp(OBSprof, BGRprof)

USE ropp_utils
USE ropp_io
USE ropp_io_types
USE ropp_fm
USE ropp_fm_copy
USE rom_num

IMPLICIT NONE

! Input/output parameters
TYPE(ROprof), intent(in)   :: OBSprof
TYPE(ROprof), intent(inout):: BGRprof

! Local variables
INTEGER            :: i
TYPE(Obs1dRefrac) :: obs_ref
TYPE(Obs1dBangle) :: obs_ben
TYPE(State1dFM)   :: bgr

REAL(wp), DIMENSION(BGRprof%Lev2b%Npoints) :: pwvp     ! Partial water vapour pressure
REAL(wp), DIMENSION(BGRprof%Lev2b%Npoints) :: pdry     ! Partial dry air pressure
REAL(wp), DIMENSION(BGRprof%Lev2b%Npoints) :: refrac   ! Refractivity
REAL(wp), DIMENSION(BGRprof%Lev2b%Npoints) :: h        ! Geometric height
REAL(wp), DIMENSION(OBSprof%Lev2a%Npoints) :: h2a       ! Geometric height (observed lev-
els)
REAL(wp), DIMENSION(BGRprof%Lev2b%Npoints) :: impact   ! Impact parameter
REAL(wp), DIMENSION(OBSprof%Lev2a%Npoints) :: impact2a ! Impact parameter (observed lev-
els)
REAL(wp), DIMENSION(BGRprof%Lev2b%Npoints) :: z_geop   ! geopot height, model levels
REAL(wp), DIMENSION(BGRprof%Lev2b%Npoints) :: zcomp_dry_inv, zcomp_wet_inv
REAL(wp)                                   :: kap1,kap2,kap3


!--- Store OBS data in Obs1dRefrac structure. Initiate refractivity values to NaN.
call ropp_fm_roprof2obs(OBSprof, obs_ref)
obs_ref%refrac = -999.0d0

!--- Store OBS data in Obs1dBangle structure. Initiate bending-angle values to NaN.
call ropp_fm_roprof2obs(OBSprof, obs_ben)
obs_ben%bangle = -999.0d0

!--- Store BGR data in a State1dFM structure (special set of units required).
!--- Model level geopotential heights are computed in the call.
BGRprof%Lev2b%press     = BGRprof%Lev2b%press*100.0d0             ! [hPa]  -> [Pa]
BGRprof%Lev2b%shum      = BGRprof%Lev2b%shum/1000.0d0             ! [g/kg] -> [kg/kg]
BGRprof%Lev2c%press_sfc = BGRprof%Lev2c%press_sfc*100.0d0         ! [hPa]  -> [Pa]
BGRprof%Lev2d%level_coeff_a = BGRprof%Lev2d%level_coeff_a*100.0d0 ! [hPa]  -> [Pa]
call ropp_fm_roprof2state(BGRprof, bgr)
! bgr%non_ideal = .true.
BGRprof%Lev2b%press     = BGRprof%Lev2b%press/100.0d0             ! convert back
BGRprof%Lev2b%shum      = BGRprof%Lev2b%shum*1000.0d0             ! convert back
BGRprof%Lev2b%geop      = bgr%geop                          ! store Lev2b geopot. height
BGRprof%Lev2c%press_sfc = BGRprof%Lev2c%press_sfc/100.0d0         ! convert back
BGRprof%Lev2d%level_coeff_a = BGRprof%Lev2d%level_coeff_a/100.0d0 ! convert back
```

```
!=== ALTERNATIVE 1: standard ROPP forward-modelling ==============================

!--- Forward-model to refractivity.
! call ropp_fm_refrac_1d(bgr, obs_ref)
! call ropp_fm_obs2roprof(obs_ref, BGRprof) ! copy forward-modelled Lev2a data to BGRprof

!--- Forward-model to bending angle.
! call ropp_fm_bangle_1d(bgr, obs_ben)
! call ropp_fm_obs2roprof(obs_ben, BGRprof) ! copy forward-modelled Lev1b data to BGRprof

!==================================================================================


!=== ALTERNATIVE 2: forward-modelling used in Level 3 processing ==================

!--- Forward-model to refractivity.
zcomp_dry_inv(:) = 1.0_wp
zcomp_wet_inv(:) = 1.0_wp
z_geop(:) = bgr%geop(:)
if (bgr%non_ideal) then
  kap1 = kappa1_comp
  kap2 = kappa2_comp
  kap3 = kappa3_comp
  call ropp_fm_compress(bgr, z_geop, zcomp_dry_inv, zcomp_wet_inv)
else
  kap1 = kappa1
  kap2 = kappa2
  kap3 = kappa3
endif
pwvp = bgr%pres * bgr%shum / (epsilon_water + (1.0_wp - epsilon_water)*bgr%shum)
pdry = bgr%pres - pwvp
refrac = kap1 * pdry * zcomp_dry_inv/ bgr%temp +     &
         kap2 * pwvp * zcomp_wet_inv/ bgr%temp**2 +  &
         kap3 * pwvp * zcomp_wet_inv/ bgr%temp
! call ropp_fm_interpol_log(z_geop, obs_ref%geop, refrac, obs_ref%refrac)    ! ORIGINAL
! call intpol1D_loglin_arr(z_geop, refrac, obs_ref%geop, obs_ref%refrac, .true.)
call intpol1D_logspline_arr(z_geop, refrac, obs_ref%geop, obs_ref%refrac, .true.)
call ropp_fm_obs2roprof(obs_ref, BGRprof)

!--- Forward-model to bending angle using an alternative 'ropp_pp_bangle_1d'.
! h = geopotential2geometric(bgr%lat, bgr%geop)                              ! ORIGINAL
! impact = (1.0_wp + 1.e-6_wp*refrac) * &                                    ! ORIGINAL
!          (h + obs_ben%r_curve + obs_ben%undulation)                        ! ORIGINAL
! call ropp_fm_abel(impact, refrac, obs_ben%impact, obs_ben%bangle)          ! ORIGINAL
h2a = geopotential2geometric(bgr%lat, obs_ref%geop)
impact2a = (1.0_wp + 1.e-6_wp*obs_ref%refrac) * &
           (h2a + obs_ben%r_curve + obs_ben%undulation)
call ropp_fm_abel(impact2a, obs_ref%refrac, obs_ben%impact, obs_ben%bangle)
where (obs_ben%bangle<-900.0_wp)
  obs_ben%weights = 0.0_wp
end where
call ropp_fm_obs2roprof(obs_ben, BGRprof)

!==================================================================================


END SUBROUTINE forward_ropp
```

References

[1] ROM SAF, The Radio Occultation Processing Package (ROPP) User Guide. Part II: Forward model and 1D-Var modules, Ref:SAF/ROM/METO/UG/ROPP/003, Version 8.0, 2015.

[2] C.P. Burrows, S.B. Healy, and I.D. Culverwell, Improvements to the ROPP refractivity and bending angle operators, ROM SAF Report 15, Ref:SAF/ROM/METO/REP/RSR/015, 2013.

[3] C.P. Burrows, S.B. Healy, and I.D. Culverwell, Improving the bias characteristics of the ROPP refractivity and bending angle operators, *Atmos. Meas. Tech.*, *7*, 3445-3458, doi:10.5194/amt-7-3445-2014, 2014.

[4] ECMWF, IFS Documentation – Cy40r1. Part III: Dynamics and numerical procedures, ECMWF, 2014.

[5] S. Schlegel, N. Korn, and G. Scheuermann, On the interpolation of data with normally distributed uncertainty for visualization, *IEEE Trans. Vis. Comput. Graphics*, *18*, 2305-2314, doi:10.1109/TVCG.2012.249, 2012.

[6] J. Eyre, Inversion of cloudy satellite sounding radiances by nonlinear optimal estimation. I: Theory and simulation for TOVS, *Q. J. R. Meteorol. Soc.*, *115*, 1001-1026, 1989.

ROM SAF (and GRAS SAF) Reports

SAF/GRAS/METO/REP/GSR/001	Mono-dimensional thinning for GPS Radio Occultation
SAF/GRAS/METO/REP/GSR/002	Geodesy calculations in ROPP
SAF/GRAS/METO/REP/GSR/003	ROPP minimiser – minROPP
SAF/GRAS/METO/REP/GSR/004	Error function calculation in ROPP
SAF/GRAS/METO/REP/GSR/005	Refractivity calculations in ROPP
SAF/GRAS/METO/REP/GSR/006	Levenberg-Marquardt minimisation in ROPP
SAF/GRAS/METO/REP/GSR/007	Abel integral calculations in ROPP
SAF/GRAS/METO/REP/GSR/008	ROPP thinner algorithm
SAF/GRAS/METO/REP/GSR/009	Refractivity coefficients used in the assimilation of GPS radio occultation measurements
SAF/GRAS/METO/REP/GSR/010	Latitudinal binning and area-weighted averaging of irregularly distributed radio occultation data
SAF/GRAS/METO/REP/GSR/011	ROPP 1D-Var validation
SAF/GRAS/METO/REP/GSR/012	Assimilation of Global Positioning System Radio Occultation data in the ECMWF ERA-Interim re-analysis
SAF/GRAS/METO/REP/GSR/013	ROPP PP validation
SAF/ROM/METO/REP/RSR/014	A review of the geodesy calculations in ROPP
SAF/ROM/METO/REP/RSR/015	Improvements to the ROPP refractivity and bending angle operators
SAF/ROM/METO/REP/GSR/016	Simplifying EGM96 undulation calculations in ROPP
SAF/ROM/METO/REP/RSR/017	Simulation of L1 and L2 bending angles with a model ionosphere
SAF/ROM/METO/REP/GSR/018	Single frequency radio occultation retrievals: impact on numerical weather prediction
SAF/ROM/METO/REP/RSR/019	Implementation of the ROPP two-dimensional bending angle observation operator in an NWP system
SAF/ROM/METO/REP/RSR/020	Interpolation artefact in ECMWF monthly standard deviation plots

ROM SAF Reports are accessible via the ROM SAF website http://www.romsaf.org